RESEARCH ARTICLE

Fast 3D Modeling of Prosthetic Robotic Hands Based on a Multi-Layer Deformable Design

Li Tian[1,2], Jianmin Zheng[1,2], Yiyu Cai[3], Muhammad Faaiz Khan Bin Abdul Halil[3], Nadia Magnenat Thalmann[1,4], Daniel Thalmann[5] and Hanhui Li[6]*

[1]Institute for Media Innovation, Nanyang Technological University, Singapore
[2]School of Computer Science and Engineering, Nanyang Technology University, Singapore
[3]School of Mechanical and Aerospace Engineering, Nanyang Technological University, Singapore
[4]MIRALab, University of Geneva, Switzerland
[5]École Polytechnique Fédérale de Lausanne, Switzerland
[6]School of Electrical and Electronic Engineering, Nanyang Technology University, Singapore

Abstract: Current research of designing prosthetic robotic hands mainly focuses on improving their functionality by devising new mechanical structures and actuation systems. Most of existing work relies on a single structure/system (e.g., bone-only or tissue-only) and ignores the fact that the human hand is composed of multiple functional structures (e.g., skin, bones, muscles, and tendons). This may increase the difficulty of the design process and lower the flexibility of the fabricated hand. To tackle this problem, this paper proposes a three-dimensional (3D) printable multi-layer design that models the hand with the layers of skin, tissues, and bones. The proposed design first obtains the 3D surface model of a target hand via 3D scanning, and then generates the 3D bone models from the surface model based on a fast template matching method. To overcome the disadvantage of the rigid bone layer in deformation, the tissue layer is introduced and represented by a concentric tube-based structure, of which the deformability can be explicitly controlled by a parameter. The experimental results show that the proposed design outperforms previous designs remarkably. With the proposed design, prosthetic robotic hands can be produced quickly with low cost and be customizable and deformable.

Keywords: Prosthetic hand; Soft materials; 3D printing

*Correspondence to: Hanhui Li, School of Electrical and Electronic Engineering, Nanyang Technological University, Singapore; hanhui.li@ntu.edu.sg

Received: July 13, 2021; **Accepted:** August 20, 2021; **Published Online:** September 28, 2021

(This article belongs to the *Special Section: 3D Printing and Bioprinting for the Future of Healthcare*)

Citation: Tian L, Zheng J, Cai Y, *et al*., 2022, Fast 3D Modeling of Prosthetic Robotic Hands Based on A Multi-Layer Deformable Design. *Int J Bioprint,* 8(1):406. http:// doi.org/10.18063/ijb.v8i1.406

1. Introduction

Designing robotic hands that mimic the general aspects of the human hand is one of the most challenging problems in robotics due to the sophisticated structure and functionality of the human hand[1]. Ever since the early dexterous Stanford/JPL hand was invented[2], there have been extensive inspiring advances in this area[3-9]. For example, Hughes *et al*.[8] proposed the conditional model that exploits the anisotropic mechanical stiffness to achieve passivity-based dynamic interactions. Particularly, replacing rigid mechanical structures with soft materials, and simplifying the hand designs are emerging trends of research in recent years[10].

From the perspective of human hand anatomy, most current robotic hands can be roughly divided into two groups: (i) rigid-body robotic hands (e.g., bone based)[3,11-15] that consist of rigid, individual structures replicating phalanges and joints, such as Shadow Dexterous Hand[3] and ACB hand[15], and (ii) soft, tissue-like hands[5,16] that are built using soft materials and actuators, among which RBO hand is the typical example[5]. These two types of robotic hands have their own advantages: rigid-body hands are reliable, sturdy, and better reflect the movement

kinematics and dynamics of the human hand, while soft robotic hands are deformable and inherently safer.

However, despite the recent notable process in soft actuators and materials, object grasping and manipulations, such as the dexterous movement of objects within the hand, remain challenging[17]. The lack of actuators equivalent in size to human hands, might be an issue to applications, such as social robotics and prosthetic hand. Besides, the customization of existing robotic hands is not easy, which means that many of them are built with predefined shapes and sizes, instead of a target given on-the-fly.

To tackle the above issues, we propose to combine the advantages of both rigid and soft robotic hands, especially the human-like mechanism of rigid hands and the deformability of soft hands. We consider human hand as the template because its kinematics and dynamics are well-studied, while the deformability provides more reliable contacts for object grasping and manipulation. We notice that most of the existing methods assume that the functionalities of human hand can be realized by a single structure (e.g. Shadow hand has a single rigid structure representing phalanges). Such an assumption actually increases the complexity of the design process and limits the candidate materials for fabrication, as various mechanical structures and actuators need to be compatible and integrated. Therefore, instead of relying on a single structure, we propose a novel multi-layer design, which highly replicates the anatomy of the human hand. Our design is composed of three layers, namely, bone, tissue, and skin, and each of them is devised for a particular purpose: the bone layer serves as the rigid, supportive structure and is attached to actuators to enable object grasping; the tissue layer is made of soft materials to guarantee the deformability of the hand; and the skin layer provides the human-like appearance.

To ensure that the proposed design can be fabricated efficiently, we exploit the advantages of three-dimensional (3D) scanning and 3D printing in rapid and adaptable fabrication[18-21]. There are a few available 3D printable materials for prosthetic hand fabrication, such as Formlabs™ Clear and Durable that have similar hardness as bones, and Formlabs™ Flexible and Elastic that is similar to human tissue in terms of flexibility. A fast template matching approach is proposed to obtain the 3D models of bones, as well as a concentric tube-based structure as the 3D model of tissues. Besides, an underactuated system, which simplifies previous complex motion control systems[14,22], is introduced in this paper.

Table 1 summarizes the differences between the proposed design and other robotic hands. To the best of our knowledge, this paper proposes the first customizable 3D printing multi-layer design for robotic hands. The proposed design allows us to fully take the advantage of soft robotic hands in deformation. We conducted extensive experiments, including the standard Feix object grasping test[26] and the trajectory test, to demonstrate that our design can effectively simulate the functionality of the human hand. Due to the deformability of our design, special objects, including extremely fragile silken tofu, smooth marbles, and tiny screw caps, can be grasped by our fabricated hand.

In summary, the contributions of this paper are threefold:

i. We propose a multi-layer robotic hand design, which combines the stability of rigid hands (via the bone layer) and the deformability of soft hands (via the tissue layer).
ii. We introduce a fast template matching method to generate the customizable 3D models of bones and tissues, which reduces the cost and complexity of robotic hand fabrication. A simplified underactuated system of 15 degrees of freedom (DOFs) and 6 degrees of actuation (DOAs) is proposed as well.
iii. The proposed tissue layer provides our robotic hand with the notable deformability, which is validated via the contact models of our robotic hand and extensive experiments. Compared with existing prosthetic robotic hand solutions, our design provides a rapid and low-cost way to fabricate a customized robotic hand with deformable tissues.

2. Materials and methods

2.1. The multi-layer deformable design

The goals of our robotic hands are dual: first, the modeling process of our robotic hands should be fast and

Table 1. Comparison of the proposed design with other robotic hands

Model	Skin	Tissue	Bone	Actuator	Joint type
Shadow hand[3]	N.A.	Rigid structures		E-motor+tendon	Rigid
EXMART hand[23]	N.A.	Rigid structures		E-motor+tendon	Dislocatable
RBO hand V2[5]	N.A.	Soft materials		Pneumatic motor	Soft continuous
Soft robotic hand	N.A.	Soft materials		Shape memory alloy	Soft continuous
Biomimetic hand[13]	N.A.	N.A.	Rigid materials	E-motor+tendon	Flexible
ACB hand[24]	N.A.	N.A.	PolyJet, resin	E-motor+tendon	Flexible
Nadine hand V4[25]	Silicone rubber	Flexible materials		E-motor+tendon	Rigid
Ours	Silicone rubber	Elastic materials	Rigid materials	E-motor+tendon	Flexible

customizable, so that we can fabricate hands of various shapes and sizes easily; second, our robotic hands should have the similar functionality of the human hand, especially in completing different grasping gestures. To this end, we propose a multi-layer deformable design of robotic hands, which mainly consists of (i) a layer of silicone skin, (ii) a layer of 3D printed tissues, (iii) a layer of 3D printed bones, and (iv) an underactuated system.

Specifically, given a real human hand as the target, we first obtained its surface model through a 3D scanner. The skin layer could be de-molded directly from the target hand to mimic the appearance of the target hand. Then, we proposed a fast template matching method to obtain the corresponding 3D bone models based on the surface model (Section 2.3). After that, an effective concentric tube structure was adopted to construct the tissue layer (Section 2.4). The tissue layer serves as the intermediate layer between the skin and bones and is made of elastic materials to allow the high deformability of our robotic hands. At last, we adopted a low-cost cable-driven system to provide our robotic hands with the mobility and stability (Section 2.6).

Compared with conventional single layer/structure robotic hands[3,13,15,25,27], our multi-layer design is more similar to human hands from the perspective of biomimetic. More importantly, as we demonstrate in the experiment section, such a deformable design is versatile for grasping objects of different shapes, textures, and materials.

2.2. Materials

For the purpose of easy customization and fabrication, all materials used in this paper are low-cost and widely accessible. Based on Young's modulus[18], we consider two 3D printing materials that have the desirable tensile strength and are compatible with the form 2 3D printer. For the bone models, we used rs-f2-gpcl-04, which is a rigid material and has 2.8 GPa tensile strength. For the tissue layer, we use an elastic 3D printable material, rs-f2-elcl-01, which has 50A shore hardness and 3.23 MPa tensile strength. The skin layer is made of silicone rubber and we chose "PlatSil Gel 10" with 10A shore hardness.

As to our actuation system, we used rubber bands as ligaments to connect bones. Nylon cables of 0.3 mm diameter and 10 lbs average breaking force were used as tendons. The servo motor, HITEC HS-5070HM, which is light (12.7 g) yet with high torque (3.6 kg/cm), was used for driving the tendons. **Figure 1** demonstrates the major materials and components of a fabricated robotic hand based on our design.

2.3. 3D modeling of bones

Modeling bones is the necessary procedure of customizing a highly biomimetic robotic hand because it provides not only the basic structure of the hand, but also the perfect guide for hand motions. However, the direct modeling of bones is difficult as they are hidden beneath the skin. Radiology methods, such as computed tomography and magnetic resonance imaging, are costly for the customized fabrication. Therefore, we propose to first obtain the surface model of the target hand through 3D scanning, and then generate the 3D mesh models of bones based on our fast template matching method.

Figure 1. Major materials and components of our robotic hands. Soft and stiff 3D printing materials were used for producing the tissues and bones, respectively. Nylon cables and rubber bands were used for simulating tendons and ligaments.

3D scanning provides a faster and more accurate way of modeling compared with traditional modeling techniques[28]. Our robotic hand design maintains more than 90% of the geometric information of a human hand through 3D scanning. Given a target hand, we scanned it with the Go! Scan™ 50 3D scanner, of which the maximum resolution is 0.5 mm. The corresponding triangle mesh-based 3D model was extracted by the VXmodel™ software. As shown in **Figure 2**, the scanned 3D model is a vivid and precise representation of the surface of the target (red dot: original point; purple dot: carpometacarpal joint; yellow dot: metacarpophalangeal joints; green dot: proximal interphalangeal joints; blue dot: distal interphalangeal joints; and orange dot: fingertips).

Next, we propose to estimate a series of geometric transformations, to match a template of 3D bone models

to the surface model. We placed landmarks on the surface model to determine the positions, orientations, and sizes of bones. As the bones have relatively fixed proportions and connections[29,30], we adjusted the surface model to make it be symmetric with respect to (w.r.t.) the xy-plane (**Figure 2**) so that the z coordinates could be ignored and this method could use 2D landmarks to reduce the complexity of labeling and computation. Based on the anatomy of the human hand, 25 landmarks were used in total, as shown in **Figure 2**. In this way, each bone was uniquely determined by 2 landmarks, and this method could construct a local 2D coordinate system for each bone, in which one of the landmarks was considered as the origin, while the other one was used as the reference to estimate the transformations. P denotes the point set of one of the template bone models, and $p = [px, py]^T \in P$ be an arbitrary point. The corresponding coordinates of p in the local coordinate system of the customized bone model, p', is calculated as follows:

$$p' = R(\theta)S(\lambda)p \tag{1}$$

where $R(\theta)$ is the rotation matrix parametrized by θ, the counterclockwise angle of rotation w.r.t. the x axis:

$$R(\theta) = \begin{bmatrix} \cos\theta & -\sin\theta \\ \sin\theta & \cos\theta \end{bmatrix} \tag{2}$$

and $S(\lambda)$ is the uniform scaling matrix with the scaling factor λ:

$$S(\lambda) = \begin{bmatrix} \lambda & 0 \\ 0 & \lambda \end{bmatrix} \tag{3}$$

θ and λ can be determined by the reference landmark. Let r' and r denote the reference landmark in the customized and the template local coordinate system, respectively. For θ, this method estimates it through the inverse trigonometric functions like arcsine, while for λ, the method considers $\lambda=(\|r'\|_2)/(\|r\|_2)$, where $\|.\|_2$ is the 2-norm.

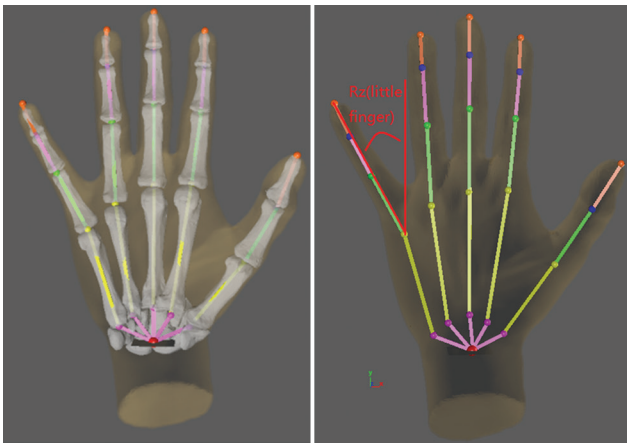

Figure 2. Hand 3D model acquired through 3D scanning and 25 landmarks and 24 segments (bottom) bones 3D model.

Before 3D printing the bones, we also put holes at the ends of them so that it could easily connect the bones with rubber bands as ligaments (refer to **Figure 3** for the details). Unlike the previous method[27] that requires the specific transformations for different landmarks, the above matching process can be applied to all 3D bone models of the template to generate the customized models. This improves the efficiency of producing customized robotic hands significantly, as the only manual operation is locating the 2D landmarks, which can be completed within a few minutes.

2.4. 3D modeling of tissue

The tissue layer is critical to the robotic hands as it helps to overcome the disadvantages of rigid, bone-only hands in object grasping. From the anatomical perspective, the soft tissues surrounding the fingers are of complex types and structures, such as subcutaneous fat and muscles. Hence, the core of modeling the tissue layer is to design a unified representational structure, which is 3D printable and deformable.

The solution to the tissue modeling problem is a novel concentric tube structure, which can be constructed in three steps described in the following: (i) hull generation. As the tissue layer cannot be scanned and modeled directly, it proposes to generate a 3D hull to determine the surfaces of the tissue layer. Note that the method already obtains the 3D mesh models of the surface and bones through the fast template matching method; therefore, it considers the surface model as the outer hull, while the bone model as the inner hull, as demonstrated in **Figure 4**. The proposed method shrinks the surface model (marked with the yellow solid curve) while expands the bone layer (marked with the red solid curve) to obtain the 2 tubes of the tissue layer. This allows the method to have a basic structure to model and 3D print the tissue layer.

(ii) Structure hollowing. This step aims at providing the basic structure with the deformability. Although the material used for the tissue layer (RS-F2-ELCL-01) is a common choice for soft structures, it is much harder than the finger tissues. Therefore, instead of using a solid structure, this method hollows the model of the tissue layer and adds supports to obtain a more elastic tube-shaped structure. Any support structure (e.g., lattice supports) could be used, and we simply use the default one provided by the Form-2 3D printer. This also brings a side benefit that this way can reduce the cost of 3D printing materials, for example, the solid design of the tissue surrounding the distal phalanx of the index finger requires about 2.9 ml material, while the hollow one only requires about 1.4 ml.

(iii) Deformation curve fitting. This method further introduces an extra parameter σ, that is, the thickness

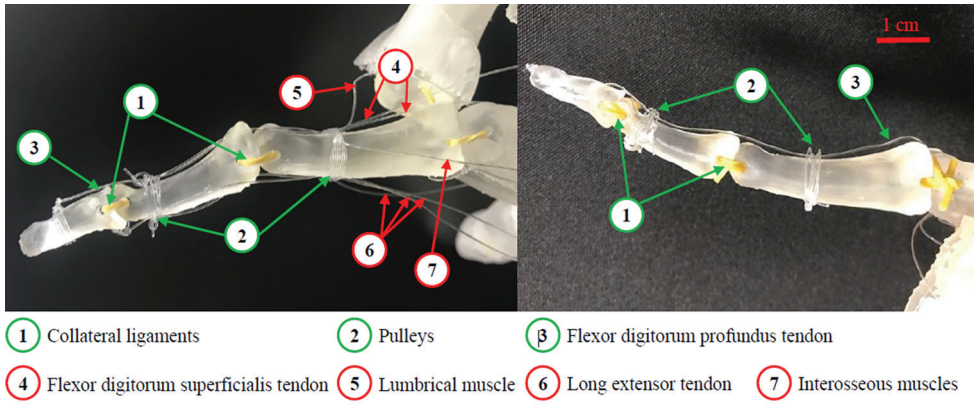

Figure 3. Demonstration of the actuation system of our previous design (left) and the simplified one used in this paper (right). The simplification is feasible due to our multi-layer design. The remaining structures are labeled in green.

of the tissue tube, to control the deformation modulus of the tissue layer. This is feasible as the larger σ is, the harder it is to deform the tissue layer. The 3D tissue model with the thickness of σ can be generated easily by shrinking the outer hull by σ, while expanding the inner hull by σ as well. In this way, the tissue layer is modeled by 2 concentric tubes, as demonstrated in **Figure 4**. To determine the optimal value of σ, this method records the curves of normal forces and contact surfaces[31] with different values of σ, and sets σ as the one with the curve being closest to that of the human finger.

Here, we summarize the steps of our fast template matching method as follows:

(i) Acquire the human hand model by 3D scanning;
(ii) Import the 3D models for bones and hand to Maya;
(iii) Manually place the landmarks of 5 fingertips;
(iv) Place the landmarks of joints;
(v) Place the hand bones based on landmarks;
(vi) Cut the hand into 5 fingers by bonding boxes;
(vii) Generate the tissue layer;
(viii) Cut each finger tissue into 3 pieces.

The codes and demonstration of the modeling process are available in the Appendix (refer to "Maya Script.zip" and "V4 3D Modeling Process.mp4"). Compared with existing robotic hand modeling method, the proposed fast template matching method provides a simple and fast way to generate 3D printable parts.

2.5. Deformation and contact model

Due to the deformability of our tissue layer, objects with various sizes can be grasped with different gestures. In this case, it is insufficient to describe the contact-mechanics model of our robot hand merely based on a single model. To tackle this problem, we propose to categorize the contacts with objects into two types based on the sizes of objects. Specifically, for grasping an object with normal size, multiple contact surfaces may be generated, and each of

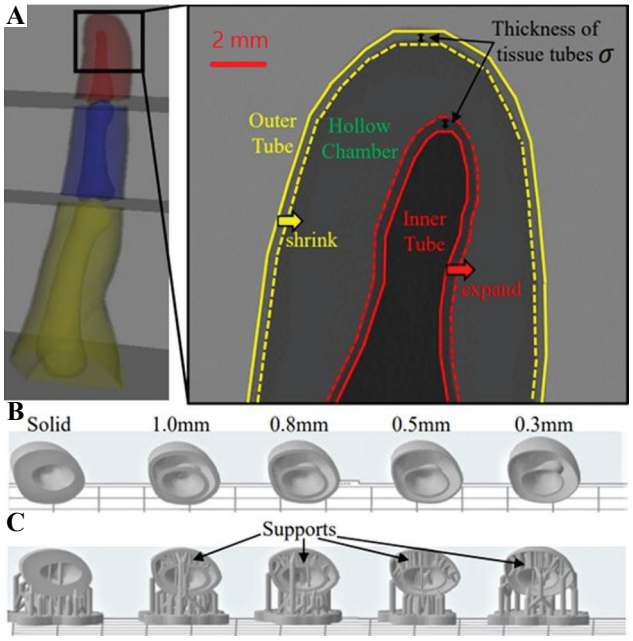

Figure 4. (A) Modeling the tissue layer as a concentric tube structure. (B) Demonstration of tissue tubes with different thicknesses. (C) Supports for stabilizing the structure.

them can be described with a nonlinear elastic model; while for a tiny object, considering the fact that the object can be enclosed by the finger, a cage based model is more suitable.

The nonlinear elastic surface model is proposed by Xydas *et al.*[32,33], which extends the Hertzian model for describing the contact surface of a soft finger as follows:

$$a = cF^{n/(2n+1)} \quad (4)$$

where c is a constant determined by the properties of the fingertip, such as the material and shape. F is the normal force pressed on the fingertip, n is the strain hardening exponent of the material, and a is the radius of the contact surface, which is assumed to be circular. However, we obverse from experiments that most contact

surfaces of the proposed design are more like ellipses, instead of standard circles. Therefore, we approximate the contact surface with an unrotated ellipse and apply Eq. (4) along its horizontal axis and vertical axis. That is, let x and y denote the horizontal axis and the vertical axis of the ellipse, and b be abbreviation of n, we record a_x and a_y w.r.t. various F, where $a_x = 1/2||x||_2$ and $a_y = 1/2||x||_2$, to estimate c_x, b_x and c_y and b_y. The experimental results validate that this nonlinear elastic model depicts the contact model of the robotic hand well: for F = [0, 4] and $\sigma = 0.4$, the estimated $a_x = 4.2960$, $b_x = 0.3497$, $a_y = 5.776$, and $b_y = 0.2203$, with the coefficient of determination (R^2) >0.94.

As to tiny objects, such as a M1 screw cap with the head diameter of 2 mm, they are far smaller than the contact surfaces generated with normal-sized objects. Object grasping in this case can be considered as forming an inescapable cage surrounding the target object, and current 2-finger/multi-finger caging theories[34,35] can be adopted for analysis. Particularly, the proposed robotic hand forms a squeezing cage[36] that the object is grasped and remains being caged when the fingers are moving closer towards the object. Furthermore, there is an interesting action that can be completed by the robotic hand, and yet has not been studied in previous caging methods: the proposed robotic hand can "press and pick up" a tiny object with the tip of a single finger. We owe this to not only the weak adhesive 3D printing material of the tissue layer, but also the friction provided by the contact cage generated by the deformation of fingertip.

2.6. The underactuated system

In this section, we described the proposed underactuated system which simulates joints, ligaments, tendons, and muscles of the human hand. Ligaments are fibrous connective tissues that connect bones to other bones and form joints. Tendons are connective tissues as well, but they are attached to muscles and bones. To mimic the dynamics of human hands, we use cables as tendons, with electric servo motors as muscles to control the motions of the finger.

Our underactuated system stems from a previous design[22], in which each of the three phalanges (i.e. the proximal, intermediate, and distal phalanx) of a finger is driven by a cable and all three cables cooperate in completing the movement. Note that there are two groups of tendons, that is, flexor tendons that bend the finger, and extensor tendons that straighten the finger. Consequently, such a design requires two groups of the driven system: one for the flexor tendons, including the flexor digitorum superficialis tendon and the flexor digitorum profundus (FDP) tendon, while the other one for the long extensor tendon, as shown in **Figure 3**. With the other two driven cables for simulating the lumbrical and interosseous muscles, eight driven cables and four motors (one motor can be shared by two cables) are used in total to control a finger.

Due to the proposed multi-layer design, the aforementioned control system can be simplified significantly. As the layers of skin and tissue are made of elastic materials, and the ligaments are resilient rubber bands, they are able to return to their original shapes automatically after being flexed, and consequently the bones are pulled back to their original positions as well (i.e., through passive movement). Thus, we removed the cables of the extensor tendon, the lumbrical and interosseous muscles. Furthermore, for the flexor tendons, we only kept the cable attached to the FDP tendon. As shown in **Figure 3**, the new underactuated system (marked in green) requires only one cable and one motor for each finger (except the thumb which uses one more motor to realize abduction and adduction). In summary, our underactuated system has 15 DOFs and 6 DOAs. This reduces the complexity and size of our system remarkably, and hence, our system can be easily installed on human arms or robotic arms.

It is noted that the proposed multi-layer structure is a universal design for robotic hand and is not limited to the above underactuated system. Highly dexterous robotic hands can be obtained with other actuation systems that adopts more actuators to achieve various object manipulations[37].

3. Experiments and results

In this section, we validated the effectiveness of the proposed design via extensive experiments. The complete experimental settings and results as well as multiple demonstration videos can be found in the Appendix.

3.1. Grasping gesture test

Following previous methods[5,13,15,25,38], we first evaluated the object grasping performance of our robotic hand with the grasp taxonomy defined by Feix *et al*.[26], which consists of 33 human grasp types. A successful grasp is defined as each static one-hand posture with which an object can be held securely. Each grasp type was tested 10 times and the success rate was used as the evaluation metric in this experiment. Two state-of-the-art robotic hands, including InMoov hand and Nadine's hand V4, were fabricated for comparison because the models and hardware specifications of InMoov hand are publicly available while Nadine's hand V4 is similar to the proposed design.

The results of the object grasping test are reported in **Figure 5**. Methods with success rates >0.8, in [0.2; 0.8] and smaller than 0.2 are labeled in green, yellow, and red, respectively. These results show that the proposed

Figure 5. Comparison of object grasping success rates of different methods. Methods with success rates ≥ 0:8, in [0.2; 0.8) and < 0.2 are labeled in green, yellow and red, respectively. The proposed robotic hand has the highest success rates for all grasping gestures.

robotic hand completes most grasp types with high success rates (rates >80%). Furthermore, the performance of the proposed robotic hand is superior to that of the InMoov hand and the Nadine's hand V4 with all 33 grasp types. Note that the number of actuators of the proposed robotic hand is equal to that of Nadine's hand V4 (i.e., 6 actuators), indicating that the success of our robotic hand mainly comes from the deformable multi-layer design.

3.2. Ablation study of the multi-layer design

To provide an insight into the effectiveness of the multi-layer design, we further conducted an ablation study in which the robotic hands with different layers were evaluated. Specifically, we performed the test of 33 grasping gestures with 3 variants of our design, including a Bone-only design, a Bone + tissue design, and a Bone + skin design.

Figure 6 demonstrates the results of the ablation study. We observe that the bone-only design failed with multiple grasp types, such as prismatic finger, extension, and writing tripod. This again validates the opinion that single layer/structure robotic hands are hard to fully imitate the ability of human hands. Nevertheless, with an extra layer of skin or tissue, the proposed design obtained the significant performance gains, for example, the success rate of the "prismatic 3 finger" type raised from below 20% to higher than 80%. The design with all three layers obtained the highest success rates. Based on these results, it can conclude that the multi-layer design is a practicable solution for robotic hands.

3.3. Deformability of the tissue layer

The deformability of the proposed robotic hands was determined by the tissue layer. To demonstrate that the proposed concentric tube structure for the tissue layer can effectively simulate the deformability of the human hand, we adopted the deformation curve as the measure of deformability and compared the proposed structure with other methods.

First, we considered two 3D printing materials for comparison, namely, the flexible material which is used by the Nadine's hand V4, and polylactic acid which is used by InMoov hand. As demonstrated in **Figure 7**, the deformation curves of these two materials are far away from those of the human finger. As mentioned above, the soft material the proposed robotic hand used is still harder than human tissues, and hence, merely using this material with the solid structure cannot achieve the desirable deformability. On the other hand, with the tube-based structure, the deformability of the tissue layer was improved greatly.

More importantly, the experimental results suggest that the proposed design can explicitly control its deformability through setting σ, the thickness of tubes. We report the deformation curves of $\sigma = [0.3\ 0.4\ 0.5\ 0.6\ 0.8]$ in **Figure 7**. It can be observed that the deformability of the proposed robotic hand is inversely proportional to σ. With $\sigma = 0.4$, we can obtain the tissue layer which has the deformation curves approximating those of the human finger.

As emphasized previously, the deformability of robotic hand is the key to grasping objects of various textures and weights. To validate this, we also conducted five experiments on grasping special objects, and include InMoov hand, Nadine Hand V3 and V4, and the proposed robotic hand without the tissue layer for comparison. The experimental results of the five experiments are summarized in **Table 2**, and further descriptions are shown in the following:

Task A: Side pinch a fragile silken tofu block. This task is introduced to demonstrate the benefits of soft and deformable materials, since rigid robotic hands without the tissue layer will crush the tofu block.

Task B: Side pinch smooth marbles with diameter of 16 mm and 24 mm. This task is designed to validate that

Table 2. Comparison of the deformability of various robotic hand designs

	InMoov hand	Nadine hand V3	Nadine hand V4	Ours without tissue	Ours
Task A: Side pinch silken tofu	x	x	✓	x	✓
Task B: Side pinch marble	x	x	✓	x	✓
Task C: Side pinch water bottle (g)	250	200	50	200	450
Task D: Fingertip pinch screws	x	x	✓	x	✓
Task E: Press and pick up M1 screw cap	x	x	x	x	✓
Maximum deformation length (x : y, in mm)	2 : 5	2 : 2	4.78 : 5.79	2 : 5	13.3 : 15.7
Sliding resistance (N)	0.96	0.93	2.16	1.18	3.43
Plane rotation resistance (N)	0.25	0.25	1.18	0.15	1.77

A design fails in a task is marked with "x," otherwise with "✓."

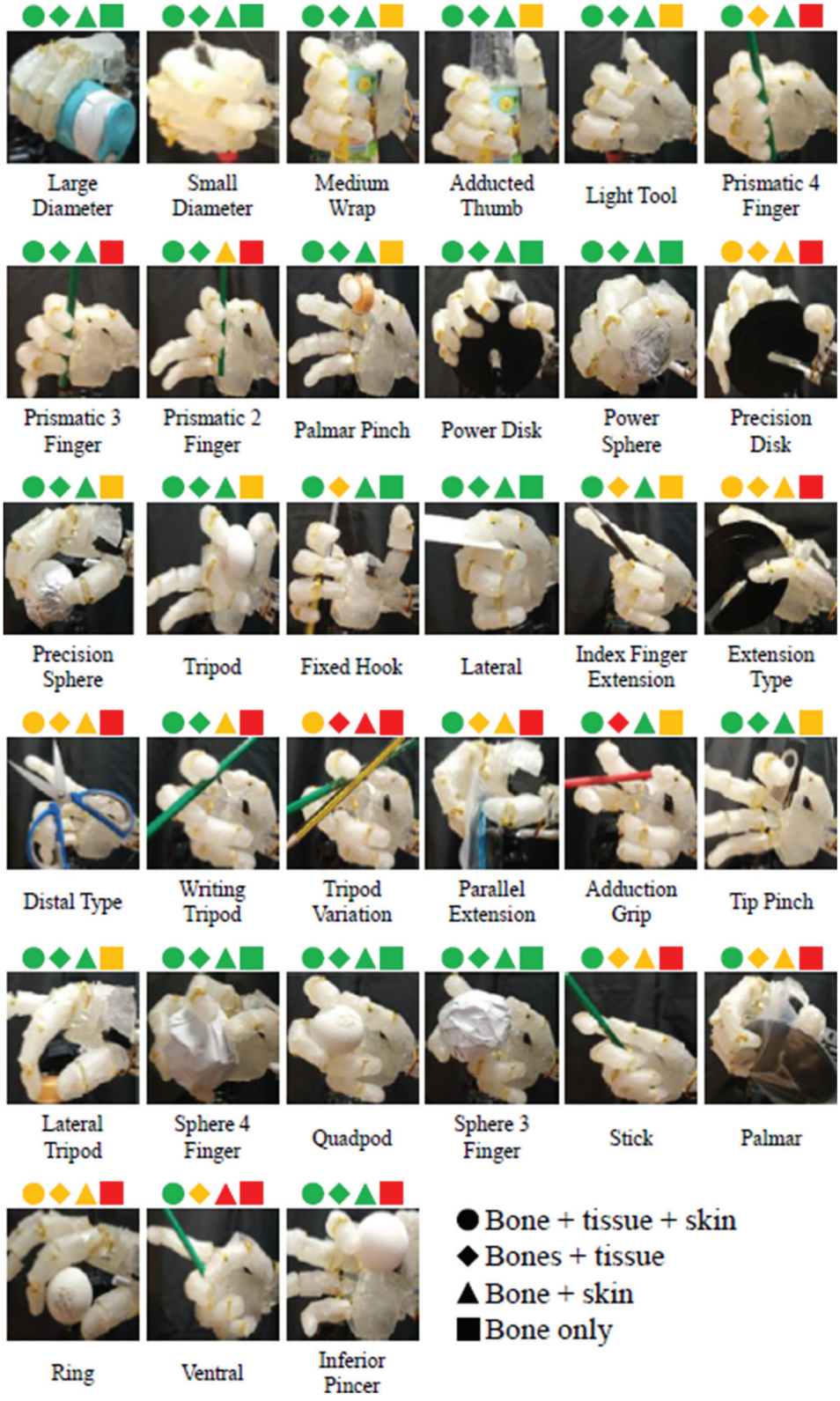

Figure 6. Comparison of object grasping success rates of the proposed robotic hands with different layers. Methods with success rates ≥0.8, in [0.2; 0.8) and < 0.2 are labeled in green, yellow, and red, respectively. This clearly validates the effectiveness of each layer in our design.

our deformable contact surfaces can provide considerable friction to grasp objects.

Task C: Side pinch a water bottle. This sub tale records the maximum weight each hand can hold. Based

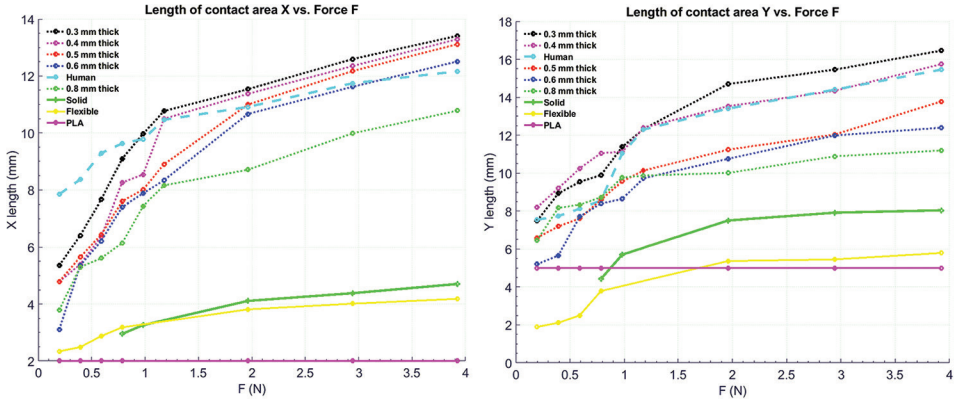

Figure 7. Graphical representation of the index finger tissue deformation under pressure.

on the results, the proposed robotic hand can pick up a water bottle of 450 g, which is larger than that of the baseline significantly.

Task D: Fingertip pinch screws. This task uses three types of screws, that is, M1, M2, and M3 in this task. We conducted this task to validate the two-finger caging model of our robotic hand. It is noted that our hand can pinch three types of screws (one for each type) simultaneously.

Task E: Press and pick up a M1 screw cap with the fingertip. The task demonstrates the single finger caging model of the proposed robotic hand. Only the proposed robotic hand and the real human hand can complete this task.

Figure 8 demonstrates several examples of the proposed robotic hand in grasping special objects. Besides, we report 3 contact-related metrics in **Table 2**, that is, the maximum deformation length, the horizontal sliding resistance, and the resistance of rotating the contact tangent plane. From these results, it can conclude that the proposed robotic hand does obtain the superior deformability compared with previous methods. Furthermore, the comparison between ours and ours without the tissue layer validates that the tissue layer is the key factor in our performance gains.

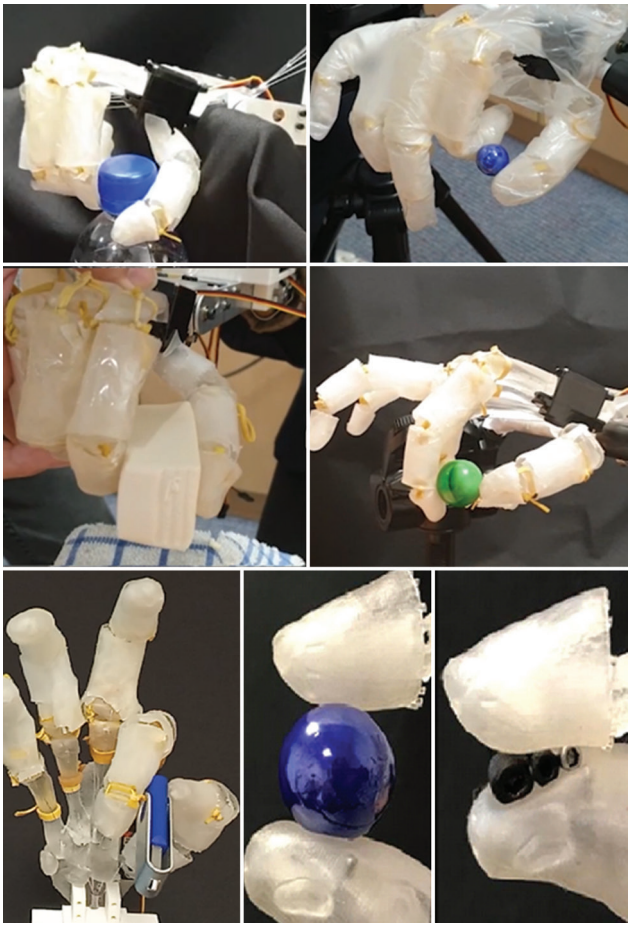

Figure 8. Demonstration of our robotic hand in pinching special objects. The proposed design can pinch (through side-pinch or fingertip-pinch) various objects stably.

3.4. Ablation study on finger design

Last but not least, we proposed to analyze the functionality of the underactuated system. First, we have compared five different solutions for joint connection in **Table 3**. The most significant advantage of using rubber bands as ligaments is that they provide the restoring force after flexion (about 3.1 N for a 4 mm rubber band), so that the proposed actuation system can remove the cables for completing extension.

Next, we recorded the trajectories of fingertips during flexion to investigate whether they can fit the trajectory of the human finger. Our system can be implemented with different configurations, for example, with different attaching knots and displacements of strings. Therefore, as demonstrated in **Figure 9**, we implemented five different designs of the system, and included the design from InMoov hand as the baseline for comparison. Configurations of these designs are summarized in **Table 4**.

Trajectories from the lateral view (i.e., the yz-plane in **Figure 2**) of the 6 designs are reported in **Figure 10**. We observed that the flexion of the baseline (Design 5) was limited as its minimum y coordinate was larger than that of the human finger by a large margin. On the contrary, all our five designs are more flexible and can better replicate the human finger. We notice that designs 2 and 6 had the similar deformation curves; therefore,

Table 3. Comparison of the joint connectors in various robotic hand designs

Connector	Type	Maximum restoring force	Force transmission
Fishing line	Ligament	0	1 Bowden cable for flexion and extension
Crocheted ligament	Ligament	0	1 cable for flexion and 1 cable for extension
Solid pin	Hinge	0	1 cable for flexion and 1 cable for extension
Flexible pin	Hinge	0	1 cable for flexion and 1 cable for extension
Rubber band (this design)	Ligament	1.5 N with 2 mm rubber band	1 cable for flexion, extension achieved via the restoring force
Rubber band (this design)	Ligament	3.1 N with 4 mm rubber band	1 cable for flexion, extension achieved via the restoring force

Table 4. Ablation study on the finger design

Design	Cable link method	Joint connector	Pulley solution	Maximum force	DIP ROM
1	Through hole and knot	4 mm rubber band	2 holes through phalanx (2 mm beneath the surface of phalanx)	18.973N	[0°, 95°]
2	Through hole and knot	4 mm rubber band	2 holes through phalanx (3 mm beneath the surface of phalanx)	8.652N	[0°, 90°]
3	DIP attaching knot	2 mm rubber band	2 holes through phalanx (1 mm beneath the surface of phalanx)	10.301N	[0°, 90°]
4	DIP attaching knot	2 mm rubber band	1 hole through phalanx (1 mm beneath the surface of phalanx) 2 nylon string windings	23.348N	[0°, 100°]
5	Inside knot	Pin joint	Hollow body	3.345N	[0°, 70°]
6	Through hole and knot	4 mm rubber band	4 nylon string windings	19.306N	[0°, 100°]

Maximum forces are measured from fingertip (in N), and ranges of motion are measured by the rotation angle of DIP (in degree).

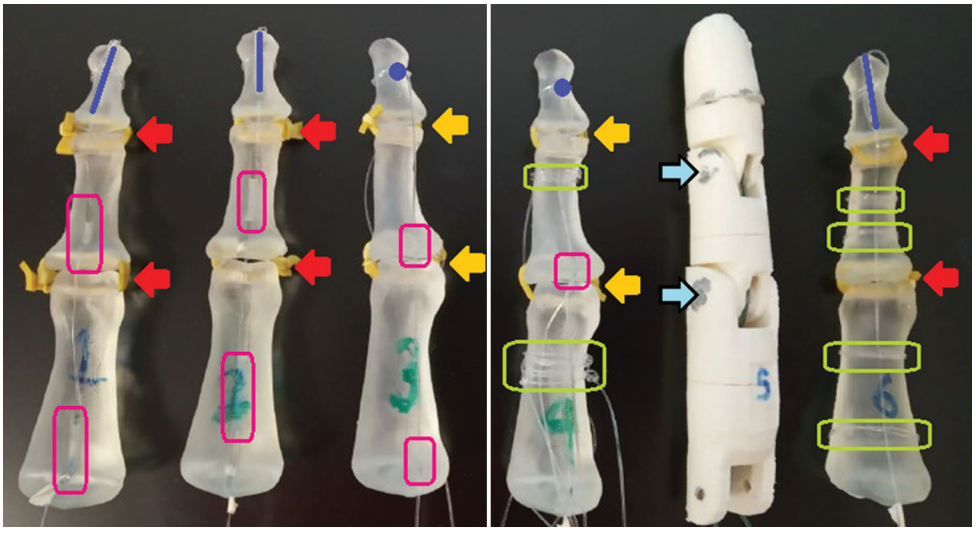

Figure 9. The 6 designs of fingers. Design 5 comes from InMoov[39]. Blue dot: driving cable and distal phalanx attaching point (knot). Blue line: through hole and knot. Yellow arrow: 2 mm thick rubber band. Red arrow: 4 mm thick rubber band. Blue arrow: pin joint. Red box: hole through phalanx. Green box: nylon string windings.

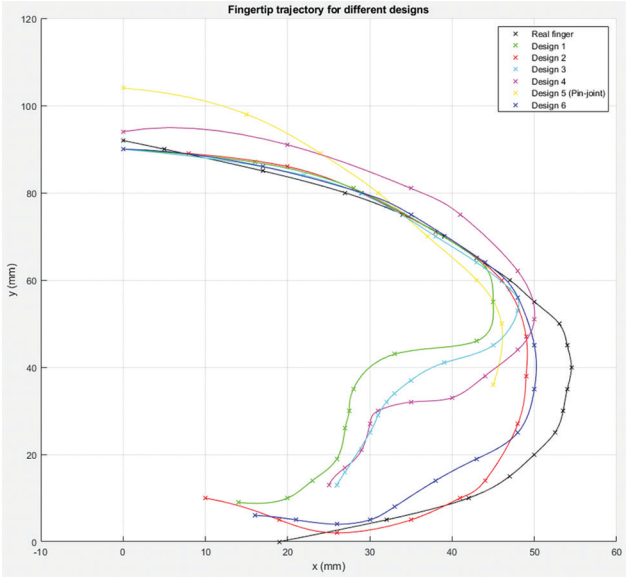

Figure 10. Fingertip trajectories during flexion with different designs of the underactuated system. These trajectories are captured from the lateral view. Design 5 is from InMoov hand.

we further measured their maximum pull strength and DIP range of motion (ROM) to decide the optimal one. With the same servomotor, the maximum pull strength of Design 6 was 19.306 N, while that of Design 2 was only 8.652 N. Design 6 also achieved the maximum DIP ROM ([0, 100]) among all variants. Therefore, we consider Design 6 as the optimal choice for implementing our underactuated system.

4. Conclusions

In this paper, we have proposed a fast and systematic method to design and fabricate customizable robotic hands which can be used as a prosthetic hand and other research purposes. The core of our method is the multi-layer design (skin-tissue-bone) inspired by the anatomy of the human hand. Our fast template matching method can generate the 3D bone models of the target hand, while our concentric tube-based structure for the tissue layer ensures that the fabricated hand is of high deformability. With the multi-layer design, we significantly reduce the cost and complexity of the actuation system. The total 3D printing and assemble time is around 12 h. The total material cost is below US$ 100. Extensive experiments with the standard object grasping types as well as with special objects demonstrate that our design is superior to previous robotic hands.

We expect that this study can provide a new baseline for fabricating robotic hands based on 3D scanning and 3D printing. In the future, we plan to add soft sensors into the hollow chamber of the tissue layer to help increase the accuracy of object grasping and manipulation. We also plan to devise an actuation system with more DOFs to complete complicated motions besides flexion and extension.

Acknowledgments

This research is supported by the National Research Foundation, Singapore under its International Research Centres in Singapore Funding Initiative, and Institute for Media Innovation, Nanyang Technological University (IMI-NTU). Any opinions, findings and conclusions or recommendations expressed in this material are those of the author(s) and do not reflect the views of National Research Foundation, Singapore.

Conflict of interest

The authors declare no known conflict of interest.

Author contributions

L T. and HH L. proposed the multi-layer design and prepared this paper. L T. and M FKBA H. conducted the experiments. JM Z, YY C., NM T., and D T. supervised this research and helped to revise this paper.

References

1. Gama Melo EN, Aviles Sanchez OF, Amaya Hurtado D, *et al*., 2014, Anthropomorphic Robotic Hands: A Review. *Ing Desarro*, 32:279–313. https://doi.org/10.14482/inde.32.2.4715
2. Salisbury JK, Roth B, 1983, Kinematic and Force Analysis of Articulated Mechanical Hands. *ASME J Mech Transm Autom Des*, 105:35–41.
3. Rothling F, Haschke R, Steil JJ, *et al*., 2007, Platform Portable Anthropomorphic Grasping with the Bielefeld 20-dof Shadow and 9-dof Tum Hand. IEEE/RSJ International Conference on Intelligent Robots and Systems, San Diego, CA, USA. https://doi.org/10.1109/iros.2007.4398963
4. Schmitz A, Pattacini U, Nori F, *et al*., 2010, Design, Realization and Sensorization of the Dexterous iCub Hand. 10th IEEE-RAS International Conference on Humanoid Robots, Nashville, TN, USA. https://doi.org/10.1109/ichr.2010.5686825
5. Deimel R, Brock O, 2016, A Novel Type of Compliant and Underactuated Robotic Hand for Dexterous Grasping. *Int J Robot Res*, 35:161–185. https://doi.org/10.1177/0278364915592961
6. Controzzi M, Clemente F, Barone D, *et al*., 2017, The SSSA-MyHand: A Dexterous Lightweight Myoelectric Hand Prosthesis. *IEEE Trans Neural Syst Rehabil Eng*, 25:459–468.

https://doi.org/10.1109/tnsre.2016.2578980

7. Piazza C, Catalano MG, Godfrey SB, *et al*., 2017, The Softhand Pro-h: A Hybrid Body-controlled, Electrically Powered Hand Prosthesis for Daily Living and Working. *IEEE Robot Autom Mag*, 24:87–101. https://doi.org/10.1109/mra.2017.2751662
8. Hughes J, Maiolino P, Iida F, 2018, An Anthropomorphic Soft Skeleton Hand Exploiting Conditional Models for Piano Playing. *Sci Robot*, 3:3098. https://doi.org/10.1126/scirobotics.aau3098
9. Liu X, Zhao Y, Geng D, *et al*., 2021, Soft Humanoid Hands with Large Grasping Force Enabled by Flexible Hybrid Pneumatic Actuators. *Soft Robot*, 8:175–185. https://doi.org/10.1089/soro.2020.0001
10. Piazza C, Grioli G, Catalano MG, *et al*., 2019, A Century of Robotic Hands. *Ann Rev Control Robot Auton Syst*, 2:1–32.
11. Gosselin C, Pelletier F, Laliberte T, 2008, An Anthropomorphic Underactuated Robotic Hand with 15 Dofs and a Single Actuator. 2008 IEEE International Conference on Robotics and Automation, Pasadena, CA, USA. https://doi.org/10.1109/robot.2008.4543295
12. Deshpande AD, Xu Z, Weghe MJ, *et al*., 2011, Mechanisms of the Anatomically Correct Testbed Hand. *IEEE/ASME Trans Mechatron*, 18:238–250.
13. Xu Z, Todorov E, 2016, Design of a Highly Biomimetic Anthropomorphic Robotic Hand Towards Artificial Limb Regeneration. 2016 Ieee International Conference on Robotics and Automation (Icra), United States, p3485–3492. https://doi.org/10.1109/icra.2016.7487528
14. Faudzi AA, Ooga J, Goto T, *et al*., 2017, Index Finger of a Human-like Robotic Hand Using Thin Soft Muscles. *IEEE Robot Autom Lett*, 3:92–99. https://doi.org/10.1109/lra.2017.2732059
15. Tasi BJ, Koller M, Cserey G, 2019, Design of the Anatomically Correct, Biomechatronic Hand. Elsevier, Netherlands.
16. Heung KH, Tong RK, Lau AT, *et al*., 2019, Robotic Glove with Soft-elastic Composite Actuators for Assisting Activities of Daily Living. *Soft Robot*, 6:289–304. https://doi.org/10.1089/soro.2017.0125
17. Billard A, Kragic D, 2019, Trends and Challenges in Robot Manipulation. *Science*, 364:8414. https://doi.org/10.1126/science.aat8414
18. Rus D, Tolley MT, 2015, Design, Fabrication and Control of Soft Robots. *Nature*, 521:467–475. https://doi.org/10.1038/nature14543
19. Liu F, Liu C, Chen Q, *et al*., 2018, Progress in Organ 3D Bioprinting. *Int J Bioprint*, 4:128.
20. Ng WL, Yeong WY, Naing MW, 2016, Polyelectrolyte Gelatin-chitosan Hydrogel Optimized for 3D Bioprinting in Skin Tissue Engineering. *Int J Bioprint*, 2:009. https://doi.org/10.18063/ijb.2016.01.009
21. An J, Chua CK, Mironov V, 2021, Application of Machine Learning in 3D Bioprinting: Focus on Development of Big Data and Digital Twin. *Int J Bioprint*, 7:342. https://doi.org/10.18063/ijb.v7i1.342
22. Tian L, Thalmann NM, Zheng J, *et al*., 2019, Design of a Highly Biomimetic and Fully-actuated Robotic Finger. 2019 IEEE Symposium Series on Computational Intelligence (SSCI), Xiamen, China. https://doi.org/10.1109/ssci44817.2019.9002870
23. Palli G, Melchiorri C, Vassura G, *et al*., 2014, The DEXMART Hand: Mechatronic Design and Experimental Evaluation of Synergy-based Control for Human-like Grasping. *Int J Robot Res*, 33:799–824. https://doi.org/10.1177/0278364913519897
24. She Y, Li C, Cleary J, *et al*., 2015, Design and fabrication of a soft robotic hand with embedded actuators and sensors. *J Mechan Robot*, 7:021007.
25. Tian L, Liu J, Thalmann NM, *et al*., 2019, Design of a Flexible Articulated Robotic Hand for a Humanoid Robot. 2019 IEEE-RAS 19th International Conference on Humanoid Robots (Humanoids), Toronto, ON, Canada. https://doi.org/10.1109/humanoids43949.2019.9035025
26. Feix T, Romero J, Schmiedmayer HB, *et al*., 2015 The Grasp Taxonomy of Human Grasp Types. *IEEE Trans Hum Mach Syst*, 46:66–77. https://doi.org/10.1109/thms.2015.2470657
27. Tian L, Magnenat-Thalmann N, Thalmann D, *et al*., 2018, A Methodology to Model and Simulate Customized Realistic Anthropomorphic Robotic Hands. Proceedings of Computer Graphics International 2018, Geneva, Switzerland, p153–162. https://doi.org/10.1145/3208159.3208182
28. Shah PB, Luximon Y, 2017, Review on 3D scanners for head and face modeling. In: International Conference on Digital Human Modeling and Applications in Health, Safety, Ergonomics and Risk Management. Springer, Berlin, Germany. https://doi.org/10.1007/978-3-319-58463-8_5
29. Alexander B, Viktor K, 2010, Proportions of Hand Segments. *Int J Morphol*, 28:755–758.
30. Li Z, Chang CC, Dempsey PG, *et al*., 2008, Validation of a Three-dimensional Hand Scanning and Dimension Extraction Method with Dimension Data. *Ergonomics*, 51:1672–1692. https://doi.org/10.1080/00140130802287280
31. Shimawaki S, Sakai N, 2007, Quasi-static Deformation

Analysis of a Human Finger Using a Three-dimensional Finite Element Model Constructed from CT Images. *J Environ Eng*, 2:56–63.
https://doi.org/10.1299/jee.2.56

32. Xydas N, Kao I, 1999. Modeling of Contact Mechanics and Friction Limit Surfaces for Soft Fingers in Robotics, with Experimental Results. *Int J Robot Res*, 18:941–950.
https://doi.org/10.1177/02783649922066673
33. Kao I, Lynch KM, Burdick JW, 2016, Contact modeling and manipulation, in Springer Handbook of Robotics. Springer, Berlin, Germany, p931–954.
https://doi.org/10.1007/978-3-319-32552-1_37
34. Rodriguez A, Mason MT, Ferry S, 2012, From Caging to Grasping. *Int J Robot Res*, 31:886–900.
https://doi.org/10.1177/0278364912442972
35. Maeda Y, Kodera N, Egawa T, 2012, Caging-based Grasping by a Robot Hand With Rigid and Soft Parts. 2012 IEEE International Conference on Robotics and Automation, Saint Paul, MN, USA
https://doi.org/10.1109/icra.2012.6224626
36. Vahedi M, van der Stappen AF, 2008, Caging Polygons with Two and Three Fingers. *Int J Robot Res*, 27:1308–1324.
https://doi.org/10.1177/0278364908098485
37. Tian L, Li H, Wang Q, *et al*., 2021, Towards Complex and Continuous Manipulation: A Gesture Based Anthropomorphic Robotic Hand Design. *IEEE Robot Autom Lett*, 6:5461–5468.
38. Zhou J, Chen Y, Li DC, *et al*., 2020, 50 Benchmarks for Anthropomorphic Hand Function-based Dexterity Classification and Kinematics-based Hand Design. 2020 IEEE/RSJ International Conference on Intelligent Robots and Systems (IROS), Las Vegas, NV, USA.
https://doi.org/10.1109/iros45743.2020.9340982
39. Langevin G, 2014, InMoov-open Source 3D Printed Life-size Robot. Available from: http://inmoov.fr/project/.
40. Tian L, Li H, Halil MF, *et al*., 2020, Fast 3D Modeling of Anthropomorphic Robotic Hands Based on a Multi-layer Deformable Design. Cornell University, New York.

Appendix

Click this link to access the supplemental materials which include the following:

(1) "Deformation Data.xlsx:" This file records the deformation tests of the tissue layer with various configurations, such as different thicknesses with and without supports and other 3D printing materials.
(2) "Maya Script.zip:" This file includes the python scripts of creating the bones and the tissue layer of the proposed design. Our generated 3D models are included as well.
(3) "V1 Demonstration.mp4:" This video file summarizes the design, fabrication, and a few experimental results of the proposed design.
(4) "V2 Grasping Test.mp4:" This video file includes examples of our grasping tests, such as selected gestures from the 33 grasp types defined in Feix *et al*., and grasping objects with different approaching methods (top approach/side approach).
(5) "V3 Ablation Study on Tissue.mp4:" This video file includes the ablation studies on the proposed tissue layer, including picking a tiny object (a screw cap, fingertip caging), and the repeat tests of several grasp gestures (with and without the tissue layer).
(6) "V4 3D Modeling Process.mp4:" This video file demonstrates how to run the python scripts to obtain the 3D models of the proposed hand.
(7) "V5 Assembly.mp4:" This video file records the complete process of assembling our 3D printed hand.

Contact author(s) if you have troubles accessing the supplemental materials. These materials are available on reasonable request.

Preprint history

A pre-print version of this article is available at https://arxiv.org/abs/2011.03742